Polygonal mounds in the Barents Sea reveal sustained organic productivity towards the P-T boundary

Tiago M. Alves[1]

[1]*3D Seismic Lab, School of Earth and Ocean Sciences, Cardiff University, Main Building, Park Place, Cardiff, CF10 3AT, United Kingdom. Email: alvest@cardiff.ac.uk*

Abstract

Three-dimensional (3D) seismic-reflection data from the Barents Sea show geometric similarities between Permian cool-water mounds and older carbonate build-ups. In detail, the Samson Dome area records the development of polygonal mounds in Upper Permian strata, at the same time a gradual drowning event took place in the Barents Sea. The presence of these polygonal mounds is interpreted to reflect: i) shallower conditions around the Samson Dome when compared to other parts of the Barents Sea; ii) earlier drowning of Upper Permian mounds towards the west and northwest into the Ottar Basin. Based on the recognition of mounds ~20 metres below the Permian-Triassic stratigraphic boundary, this paper proposes for the first time that shallow areas of the Barents Sea, such as the Samson Dome, witnessed sustained organic productivity until the onset of the P-T extinction event.

Keywords: Pangaea; Barents Sea; carbonate build-ups; Upper Permian mounds; P-T boundary.

Introduction

Continental margins of the Arctic Sea were affected by multiple tectonic events during rifting and subsequent break-up of the Pangaea supercontinent (Faleide et al., 1984; 1993; Glørstad-Clark

et al., 2010). As a result, polygonal carbonate build-ups grew on active structural highs of the Barents Sea prior to the development of isolated (cool-water) reefs in the latest Palaeozoic (Elvebakk et al., 2002; Colpaert et al., 2007) (Fig. 1). This shift from warm- to cool-water conditions was accompanied by important lithological changes. Carboniferous-Lower Permian build-ups are carbonate-rich and alternate with evaporites and dolomitic sediments (Blendinger et at, 1997; Rafaelsen et al., 2008). In contrast, Upper Permian sediments comprise a mixture of siliciclastics, cherts and carbonates accumulated during a long term sea-level rise (Nøttvedt et al., 1993).

On Svalbard, detrital banks of locally derived limestones with bryozoan-echinoderm-spicule fragmental debris, crinoids, sponges and brachiopods, comprise the majority of the Upper Permian Kapp Starostin Formation (Blendinger et al., 1997; Ehrenberg et al., 2001). Lacking the sediment-baffling or binding mode of accumulation typical of the Upper Carboniferous-Lower Permian build-ups (Malkowski and Hoffman, 1979; Wignall et al., 1998; Ehrenberg et al., 2001; 2010), regional seismic and borehole data nevertheless showed these detrital banks as capable of forming reliefs of 10s of metres on the Permian seafloor (Ehrenberg et al., 1998). They are intercalated with siliceous shales and more marginal carbonates and clastics (Nilson et al., 1996). Further south on the Finnmark Platform, Mid-Upper Permian build-ups are locally developed and interpreted as similar to those formed in Upper Permian strata of East Greenland (Gérard & Buhrig, 1990). Their geometries and extent in the Barents Sea, however, have not been investigated using a combination of high-quality 3D seismic and borehole data.

This paper focuses on a region ~150 km to the northwest of Finnmark, Northern Norway (Figs. 1a and 1b). It documents, for the first time, the generation of ~150m-thick polygonal mounds in the Central Barents Sea during the Late Permian. These mounds grew away from the more sheltered Finnmark Platform and are that are geometrically similar to older Carboniferous build-ups (Fig. 1a). Their identification suggests sustained organic productivity in shallow parts of the Barents Sea until very close to the P-T extinction event (252 Ma; Shen et al., 2011).

Data and methods

This work uses three-dimensional (3D) seismic data and regional 2D profiles across 1160 km^2 of the Barents Sea (Figs 1a and 1b). The dataset images a salt anticline, the Samson Dome, of yet undetermined age (Figs. 1a and 1b). The 3D seismic volume has a bin spacing of 12.5 x 25 m, a 4 ms vertical sampling window, and was acquired by a 10 x 6000 m array of streamers. Data processing included signal resampling, TAU-P linear noise attenuation, TAU-P domain deconvolution and zero-phase conversions. Pre-stack time migration used the Kirchhoff algorithm. As a result, any velocity-derived seismic artefacts were processed out of the seismic volume. Time-depth conversions were undertaken using a V_p-wave velocity of 5800 m/s for Upper Permian mounds, and 6600 m/s for Carboniferous-Lower Permian strata, based on wells 7121/1-1 R and 7124/3-1 (Figs. 1a and 2). Vertical seismic resolution approaches 60 m.

Regional 2D profiles were used to tie stratigraphic data from two exploration wells to the 3D seismic volume (Figs. 1a and 2). Well 7124/3-1 is located 36 km to the south of the 3D seismic volume. Well 7121/1-1R is located on the Loppa High c. 105 km to the west of the Samson Dome (Figs. 1a, 2a and 2b). Well 7224/7-1 was drilled on the Samson Dome without crossing Permian strata.

Biostratigraphy constraints are robust for the Carboniferous-Early Permian, but information for Upper Permian strata are based on sparser outcrop and borehole data (Larsen et al., 2002). Nevertheless, Ehrenberg et al. (1998) and Glørstad-Clark et al. (2010) identified a maximum-flooding surface (MFS) at the top of Permian strata in the Barents Sea (Glørstad-Clark et al., 2010) (Figs. 2, 3 and 4). The MFS was used by Ehrenberg et al. (2001) to correlate outcrops in Svalbard with wells 7128/6-1 and 7128/4-1 on the Finnmark Platform. Over the Samson Dome, the top Permian MFS is a negative to transparent continuous reflection observed ~10 ms (25-30 m) above Horizon 1 (Figs. 3 and 4).

Regional geological setting

On the Loppa High, Carboniferous build-ups were long-lived (~35 Ma), polygonal, and of high depositional relief (< 420 m) (Elvebakk et al., 2002) (Fig. 1a). They were also relatively static, changing laterally into evaporites and dolomites in adjacent basin depocentres (Ehrenberg et al., 1998) (Fig. 1c). In contrast to the Carboniferous, large isolated carbonate build-ups of Early Permian (Artinskian) age became detached from shelf areas on the Finnmark Platform (Colpaert et al., 2007), but not on the Loppa High where they preserved a polygonal mosaic of laterally extensive ridges (Elvebakk et al., 2002). Isolated build-ups on the Finnmark Platform record a change from photozoan assemblages below the Artinskian (unit L-7), to heterozoan biota above (unit L-8) due to a shift from warm- to cool-water conditions (Beauchamp and Desrochers, 1997; Stemmerik, 1997; Ehrenberg et al., 1998; Beauchamp and Baud, 2002) (Table 1). Significantly, rapid flooding of isolated carbonate build-ups occurred after the Kungurian throughout the Barents Sea, in contrast to the regression recorded in global sea-level curves, and at the top of the Upper Permian interval analysed in this paper (Fig. 3).

Upper Permian detrital banks formed by locally derived bryozoan-echinoderm-spicule fragmental debris have thus been identified on Finnmark and Svalbard (Ehrenberg et al., 1998; 2010). They are ?Kungurian to Late Permian in age, and comprise cold-water 'hyalosponge-bryonoderm' assemblages part of unit L-9 (Beauchamp, 1993; 1994) (Fig. 3 and Table 1). At a regional scale, this same L-9 unit marks the closure of the Uralian seaway, which extended as far south as the tropical regions of the Pre-Caspian basin.

On the Samson Dome, well 7224/7-1 crossed a thick (~600 m) succession of Lower Triassic strata above a Top Permian maximum-flooding surface (MFS) (Fig. 2a). On the Loppa High, well 7121/1-1 R drilled a 2007 m thick Palaeozoic section of silicified limestones, limestones, dolomitic limestones and dolomites, with minor amounts of chert, siltstones and anhydrites (Larsen et al.,

105 2002) (Figs. 2 and 4). As a comparison, well 7124/3-1 drilled only 604 m of Palaeozoic strata (Figs.
106 2a, 2b and 4). Upper Permian strata in well 7124/3-1 comprise limestone, spiculitic (chert-
107 dominated) and shaley intervals.

108 The contact between Upper Permian strata and overlying shales is apparently conformable and
109 occurs ~20 m below a sharp increase in gamma-ray values as the top Permian MFS is crossed (Figs.
110 4 and 5). The P-T boundary *per se* occurs near the base of the high gamma-ray interval shown in
111 Fig. 4. On Svalbard, the top of Upper Permian spiculites was suggested by Wignall et al. (1998) and
112 Mørk et al. (1999) to precede the Permian-Triassic (P-T) boundary by ~ 10 m.

113

114 **Geometry of Carboniferous polygonal build-ups**

115

116 Carboniferous polygonal build-ups have long and short ridges, and show a predominant
117 northwest strike for the longest ridges in Horizon 5 (Figs. 6 and 7). In cross-section, their width is
118 typically 250–750 m for a length of < 3.0 km. More distal facies are interpreted northwest of the
119 Samson Dome where build-ups are scarce (Figs. 7a and 7b).

120 Polygonal build-ups change their geometry from smooth to steep, asymmetric features near the
121 Carboniferous-Permian boundary i.e., below Horizon 4 (Figs. 5, 6 and 7b). Similarly to the Loppa
122 High, the steeper flanks of Carboniferous build-ups identified on the Samson Dome face seawards
123 to the northwest (Fig. 7b). However, build-ups change orientation from Horizon 6 to Horizon 4
124 (Fig. 7). Horizon 4 shows a series of linear build-ups around the Samson Dome and small isolated
125 build-ups to the southeast and east (Fig. 7b). In cross-section, the width of these linear build-ups is
126 typically 200-300 m, with a maximum of ~1.5 km (Fig. 5). Small isolated build-ups are observed
127 together with irregular polygonal features (Figs. 6 and 7c). These features are interpreted as small
128 patches of isolated build-ups that continued their development in risen parts of older carbonate
129 edifices.

130

Isolated build-ups of Early Permian age

A major change in geometry is recorded above Horizon 4 with the appearance of isolated (cool-water) build-ups (Fig. 8a). This change was interpreted by Ehrenberg et al. (1998) as marking a shift from photozoan (sunlight-dependent) to heterozoan (mainly sunlight-independent) biota at the L-7/L-8 boundary (Table 1). In Figure 8a, a two-way time (TWT) structural map for Horizon 3 demonstrates the wide distribution of isolated build-ups in the study area. Using velocity (V_p) data from well 7121/1-1 R, an average thickness of ~575 m was calculated for the isolated build-ups. A maximum thickness of ~739 m was observed to the southeast of the Samson Dome (Figs. 8a and 9a).

Blendinger et al. (1997) and Ehrenberg et al. (1998) showed Lower Permian build-ups to comprise carbonate cements and bryozoan-echinoderm wackestones to grainstones. The associated change in biota across the L-7/L-8 boundary resulted from a decrease in water temperature, but with the recognised caveat that biota and lithologies very similar to L-8 occur in thin, transgressive intervals in L-7 and L-6 (Ehrenberg et al., 1998). Alternatively, the latter authors explain the biotic change at the L-7/L-8 boundary as relating to a relative rise in sea level, which would have eliminated barriers to oceanic circulation promoting the establishment of cool-water currents across the Finnmark platform. Details of typical depositional environments in L-7 and L-8 are provided in Table 1.

Upper Permian polygonal mounds

The main difference between the study area, the Finnmark Platform and the Loppa High, is the return of mounds with polygonal geometries in the Late Permian, this time with a characteristic distribution to the east and southeast of the Samson Dome (Figs. 5, 6 and 8b). Morphological data show that Upper Permian polygonal mounds are ~151-m thick on average (Fig. 9a). Upper Permian

mounds show low-amplitude, parallel to sub-parallel seismic reflections with moderate thickening towards their flanks (Figs. 5 and 6). This character suggests the presence of interbedded shales in the successions imaged around the Samson Dome, with polygonal features comprising localised spiculitic-carbonate mounds and detrital banks similar to those documented on Svalbard (Ehrenberg et al., 2001) (Figs. 5, 8b and 8c).

The maps in Figs. 9b and 9c highlight the shifts in the position of carbonate build-ups and Upper Permian mounds. The early settlement of carbonate build-ups above Horizon 6 was followed by the drowning of some 90% of these same edifices at Horizon 4, with linear build-ups forming on the margins of the Samson Dome. This same event coincides with a highstand period that drowned most of the polygonal build-ups generated in the Late Carboniferous. However, some surviving pinnacle-like build-ups were kept over the large edifices observed in Horizon 4 (Figs. 6 and 7c). These pinnacle build-ups later formed the base for Lower Permian mounds, which shifted location by a few 100's of metres to <1 km in regressive sea-level conditions (Figs. 9b and 9c). Upper Permian mounds also show lateral shifts of 100's of metres, being concentrated in the region to the southeast of the Samson Dome as we cross Horizon H1 into the top Permian MFS (Figs. 6 and 9c).

Discussion and conclusions

The interpreted data favours two explanations for sustained organic productivity into the P-T boundary. The first explanation takes into account a combination of halokinesis and late Variscan tectonics, necessary to maintain a relatively shallow seafloor over the Samson Dome. The main tectonic event affecting the Barents Sea during the Late Carboniferous-Permian is recorded in the form of a regional Kungurian unconformity (Fig. 3). However, this unconformity is not identified on the Samson Dome, with polygonal mounds occurring above Horizon 2 until the top Permian MFS (~20 m above Horizon 1) drowned all carbonate edifices (Figs. 4 and 5). Regardless of the importance of tectonics as a controlling factor on Late Permian deposition, Schlager and Purkis

(2015) suggested as primary cause for the generation of polygonal features on carbonate platforms a tendency for biotic self-organization. The link between karst morphology and overlying reef patterns was deemed unconvincing for a significant number of examples, particularly those on a substrate of tower karst with high relief. Instead, an alternative pathway to reticulate reefs may be the colonization of reticulate hydrodynamic bedforms by reef builders (Schlager and Purkis, 2015). This latter postulate is supported in this work, with Upper Permian mounds around the Samson Dome forming polygonal patterns on an irregular seafloor, which they were able to colonise in an organised way (Figs. 9b, 9c and 10).

Ehrenberg et al. (1998) showed that Upper Permian strata comprise detrital banks of calcareous spiculite and subordinate mudstone with nodular to lensoid fabrics and abundant laminations. Detrital banks formed biostromes and, lacking the binding mode characteristic of the older Carboniferous build-ups, they are assumed to have nucleated in a spicule-covered seabed in areas of favourable topography and nutrient supply, after which enhanced carbonate production was reinforced by bioherm relief (Ehrenberg et al., 1998). As the 3D seismic data interpreted in this work has been processed to exclude velocity artefacts, and Upper Permian mounds have a significant relief (151 m on average), they are interpreted to comprise authochtonous carbonate mounds developed in quiet, and relatively deep waters with variable contribution from baffled, bound or trapped spiculitic grains (see Pratt, 2000 and Wood, 2001). In addition, mounded structures with bright amplitude seen on seismic at top Permian level are likely to be porosity anomalies within spiculitic sediment, enhancing any biologically constructed build-ups and banks with ~150-m relief (Figs. 5, 8b and 8c).

A second explanation assumes an established balance between relative sea-level, accommodation space and tectonic movements for a period of time as long as 55-60 Ma. In this case, the presence of relative thick evaporites above the Variscan structures resulted in a smoother seafloor, hindering a closer control of basement faults upon mound growth - a setting that is markedly distinct from the Loppa High (e.g. Elvebakk et al., 2002). As the interpreted mounds

present depositional thickening relative to adjacent strata that is typical of carbonate build-ups and mounds in multiple geological settings (Bosence and Bridges 1995; Burgess et al., 2013), this paper proposes the region to the southeast of the Samson Dome to have been shallow enough to support the growth of polygonal mounds until the Late Permian. As suggested by Gérard and Buhrig (1990), the polygonal mounds appear to rest on top of a silicified seafloor, anticipating the sudden arrival of Triassic clastic material to the Barents Sea. In such a setting, the persistence of self-organised carbonate mounds beyond the Kungurian unconformity proves that organic productivity was maintained, albeit at a local scale, on the northern margin of Pangea. The Permian mounds interpreted in this work also demonstrate the extent of carbonate deposition beyond the Finnmark Platform above persistent structural highs. As a corollary, it is suggested that structures similar to the Samson Dome prevented exposure, or drowning, of Upper Permian mounds in the Barents Sea until very close to the P-T boundary.

Acknowledgments

The authors acknowledge the BG Group and Jonathan Turner for the use of the data in this paper. K. Omosanya, S. Johansen and the Norwegian University of Science and Technology (NTNU) are acknowledged for providing 2D and borehole data. We thank Associate Editor Dan Bosence, D. Pollit and P. Gutteridge for their constructive comments. This paper used Schlumberger's Petrel®.

REFERENCES

Beauchamp , B., 1993. Carboniferous and Permian reefs of the Sverdrup Basin, Canadian arctic islands. In *Arctic Geology and Petroleum Potential* (T.O. Vorren, E. Bergsaker, Ø.A. Dahl-Stamnes, E. Holter, B. Johansen, E. Lie, T.B. Lund, eds). *Norwegian Petroleum Society (NPF), Special Publication*, **2**, Elsevier, Amsterdam, 217 – 241.

Beauchamp, B., 1994. Permian climatic cooling in the Canadian Arctic. *GSA Sp. Papers*, **288**, 229-246.

235 Beauchamp, B. and Baud, A., 2002. Growth and demise of Permian biogenic chert along northwest
236 Pangea: evidence for end-Permian collapse of thermohaline circulation. *Palaeog., Palaeoclim.,*
237 *Palaeoec.*, **184**, 37-63.
238 Beauchamp, B. and Desrochers, A., 1997. Permian warm- to very cold-water carbonates and chert
239 in the Sverdrup Basin–Barents Sea area, northwestern Pangea. In *Cool-water Carbonates* (N.P.
240 James, J. Clark, eds). *Soc. Econ. Paleont. Mineral., Special Publication*, **56**, 349–364.
241 Blendinger, W., Bowlin, B., Zijp, F.R., Darke, G. and Ekroll, M., 1997. Carbonate build-up flank
242 deposits: an example from the Permian (Barents Sea, northern Norway) challenges classical facies
243 models. *Sed. Geol.*, **112**, 89-103.
244 Bosence, D.W.J. and Bridges, P.H., 1995. A review of the origin and evolution of carbonate mud-
245 mounds. In *Carbonate Mud-Mounds: Their Origin and Evolution* (C.L.V. Monty, D.W.J.
246 Bosence, P.H. Bridges, B.R. Pratt eds). *Inter. Assoc. Sed., Special Publication*, **23**, 3-10.
247 Burgess, P.M., Winefield, P., Minzoni, M. and Elders, Ch., 2013. Methods for identification of
248 isolated carbonate buildups from seismic and reflection data. *AAPG Bull.*, **97**, 1071-1098.
249 Colpaert, A., N. Pickard, Mienert, J., Henriksen, L.B. , Rafaelsen, B. and Andreassen, K., 2007. 3D
250 seismic analysis of an Upper Palaeozoic carbonate succession of the Eastern Finnmark Platform
251 area, Norwegian Barents Sea. *Sed. Geol.*, **197**, 79-98.
252 Ehrenberg, S.N., McArthur, J.M. and Thirlwall, M.F., 2010. Strontium isotope dating of spiculitic
253 Permian strata from Spitsbergen outcrops and Barents Sea well-cores. *J. Petrol. Geol.*, **33**, 247-
254 254.
255 Ehrenberg, S.N., Nielsen, E.B., Svånå, T.A. and Stemmerik, L. 1998. Depositional evolution of the
256 Finnmark carbonate platform, Barents Sea: Results from wells 7128/6-1 and 7128/4-1. *Norsk*
257 *Geol. Tidsskrift*, **78**, 185-224.
258 Ehrenberg, S.N., Pickard, N.A.H,. Henriksen, L.B., Swaanaa, T.A., Gutteridge, P. and Macdonald,
259 D.I.M., 2001. A depositional and sequence stratigraphic model for cold-water, spiculitic strata

based on the Kapp Starostin Formation (Permian) of Spisbergen and equivalent deposits of the Barents Sea. *AAPG Bulletin*, **85**, 2061-2087.

Elvebakk, G., Hunt, D.W. and Stemmerik, L., 2002. From isolated build-ups to build-up mosaics: 3D seismic sheds new light on upper Carboniferous–Permian fault controlled carbonate build-ups, Norwegian Barents Sea. *Sed. Geol.*, **152**, 7-17.

Faleide, J.I., Gudlaugsson, S.T. and Jacquart, G., 1984. Evolution of the western Barents Sea. *Mar. Petrol. Geol.*, **1**, 123–150.

Faleide, J.I., Vågnes, E. and Gudlaugsson, S.T., 1993. Late Mesozoic-Cenozoic evolution of the south-western Barents Sea in a regional rift-shear tectonic setting. *Mar. Petrol. Geol.*, **3**, 186-214.

Gérard, J. and Buhrig, C., 1990. Seismic facies of the Permian section of the Barents Shelf, analysis and interpretation. *Mar. Petr. Geol.*, **7**, 234-252.

Glørstad-Clark, E., J.I. Faleide, B.A. Lundschien and J.P. Nystuen, 2010. Triassic seismic sequence stratigraphy and paleogeography of the western Barents Sea area. *Mar. Petrol. Geol.*, **27**, 1448-1475.

Gudlaugsson, S.T., Faleide, J.I., Johansen, S.E. and Breivik, A.J., 1998. Late Palaeozoic structural development of the South-western Barents Sea. *Mar. Petrol. Geol.*, **15**, 73-102.

Haq, B.U. and Schutter, S.R., 2008. A chronology of Paleozoic Sea-Level changes. *Science*, **322**, 64-68.

Larssen, G.B., Elvebakk, G., Henriksen, L.B., Kristensen, S.-E., Nilsson, I., Samuelsberg, T.J., Svånå, T.A., Stemmerik, L. and Worsley, D., 2002. Upper Palaeozoic lithostratigraphy of the Southern Norwegian Barents Sea. http://www.npd.no/Norsk/Produkter+og+tjenester/Publikasjoner/Oversikt+sokkelpublikasjoner/npd+bulletin. htm. 76 pp., 63 figs., 1 tbl.

Malkowski, K. and Hoffman, A., 1979. Semi-quantitative facies model for the Kapp Starostin Formation (Permian), Spitsbergen. *Acta Palaeont. Pol.*, **24**, 217–230.

285 Mørk, A. and Elvebakk, G., 1999. Lithological description of subcropping Lower and Middle
286 Triasic rocks from the Svalis Dome, Barents Sea. *Polar Res.*, **18**, 83-104.
287 Nilson, I., Mangerud, G. and Mørk, A., 1996. Permian stratigraphy of the Svalis Dome, south-
288 western Barents Sea. *Norsk Geol. Tids.*, **76**, 127-146.
289 Nøttvedt, A., Cecchi, M., Gjelberg, J.G., Kristensen, S.E., Lonoy, A., Rasmussen, A., Rasmussen,
290 E., Skott, P.H., van Veen, P.M., 1993. Svalbard-Barents Sea correlation: a short review. In:
291 Vorren, T., Bergsager, E., Dahl-Stamnes, Ø., Holter, E., Johansen, B., Lie, E., Lund, T. (Eds.),
292 Arctic Geology and Petroleum Potential. Norwegian Petroleum Society (NPF), Special
293 Publication, Elsevier, Amsterdam, **2**, 363-375.
294 Pratt, B.R., 2000. Microbial contribution to Reefal mud-mounds in ancient deep-water settings:
295 evidence from the Cambrian. In *Microbial Sediments* (R. Riding, S.M. Aramik, eds). *Springer-*
296 *Verlag, Berlin*, 282-293.
297 Rafaelsen, B., Elvebakk, G., Andreassen, K., Stemmerik, L., Colpaert, A. and Samuelsberg, T.J.,
298 2008. From detached to attached carbonate buildup complexes — 3D seismic data from the upper
299 Palaeozoic, Finnmark Platform, southwestern Barents Sea. *Sed. Geol.*, **206**, 17-32.
300 Shell Exploration and Production, 1995. Standard Legend. Shell International Exploration And
301 Production B.V., The Hague, 212 pp.
302 Shen, S-Z., Crowley, J.L., Wang, Y., Bowring, S.A., Erwin, D.H., Sadler, P.M., Cao, C., Rothman,
303 D.H., Henderson, C.M., Ramezani, J., Zhang, H., Shen, Y., Wang, X., Wang, W., Mu, L., Li, W.,
304 Tang, Y., Liu, X-l., Liu, L., Zeng, Y., Jiang, Y. and Jin, Y., 2011. Calibrating the End-Permian
305 Mass Extinction. *Science*, **334**, 1367-1372.
306 Stemmerik, L., 1997. Permian (Artinskian - Kazanian) cool-water carbonates in North Greenland,
307 Svalbard and the western Barents Sea. In *Cool-water Carbonates* (N.P. James, J. Clark, eds). *Soc.*
308 *Econ. Paleont. Mineral., Special Publication*, **56**,349–364.

Wignall, P.B., Morante, R. and Newton, R., 1998. Permo-Triassic transition in Spitsbergen: $\delta^{13}C$ chemostratigraphy, Fe and S geochemistry, facies, fauna and trace fossils. *Geol. Mag.*, **135**, 47-62.

Wood, R., 2001. Are reefs and mud mounds really so different? *Sed. Geol.*, **145**, 161-171.

Figure Captions

Figure 1 – (a) Map of the Barents Sea depicting the location of geological features mentioned in the text and the interpreted 3D seismic volume. (b) Two-way time (TWT) structure of the Mid Jurassic Major Sequence Boundary (MSB) highlighting the geometry of the Samson Dome, the locations of selected profiles shown in the paper and the locations of wells 7124/3-1 and 7224/7-1. (c) Schematic dip section across the Loppa High illustrating the control of basement structures on buildup location as inferred by Elvebakk et al. (2002). tA - top Artinskian; iK - intra-Kasimovian; IM - intra-Moscovian ; IB - intra-Basement. The regional map in (a) is modified from Faleide et al. (2008), Gudlaugsson et al. (1998) and Glørstad-Clark et al. (2010).

Figure 2 – a) North-South 2D seismic profile crossing the Samson Dome showing the main structural features in the study area and interpreted seismic stratigraphic intervals. b) Composite 2D seismic profile crossing the region south of the Samson Dome and Loppa High illustrating the main seismic-stratigraphic boundaries interpreted in the Barents Sea. The location of the 2D profiles and wells is shown in Figure 1a.

Figure 3 - Correlation panel amongst the interpreted seismic units, stratigraphic information from Larsen et al. (2002), Glørstad-Clark et al. (2010) and published global sea-level curves for the Late Devonian-Early Tertiary time periods (Haq and Schutter, 2008). See Figure 1a for the location of

the two seismic sections. Well data is courtesy of the Norwegian Petroleum Directorate (NPD). Vertical exaggeration approaches 10x on the seismic sections.

Figure 4 - a) Correlation panel between stratigraphic units in the study area, and wells 7121/1-1 R and 7124/3-1. Main seismic surfaces (Horizons H1 to H6) interpreted in this work are highlighted in the panel. The abbreviations used to describe borehole lithologies are based on the Shell Exploration and Production (1995) standard borehole legend.

Figure 5 - a) and b) Zoomed seismic sections across Carboniferous-Permian units in the Samson Dome area. The sections highlight the acoustic character of the P-T boundary and Upper Permian mounds. Note the vertical scale of 100 ms shown next to the imaged mounds (see insets). Figure 1b shows the location of the seismic sections. Vertical exaggeration = 5x.

Figure 6 – North-South seismic section highlighting the geometry of isolated build-ups and mound systems across the study area. a) Uninterpreted seismic section imaging Carboniferous-Lower Triassic strata in the study area. b) Interpreted seismic section highlighting the main seismic-stratigraphic boundaries (and units) observed across the Samson Dome area. Note the tabular to pinnacle-like shapes of Late Carboniferous build-ups and their different sizes in Horizons 3 to 6. Vertical exaggeration = 10x.

Figure 7 – TWT structure maps highlighting the geometry of carbonate build-ups from Horizon H6 to H4. a) Reveals the onset of polygonal build-ups at the base of the Falk Formation, with deeper basins being devoid of build-ups. b) Shows sets of developed polygonal build-ups at the base of the Ørn Formation, Late Carboniferous. c) Reflects the drowning and demise of polygonal build-ups at the start of the Permian. Vertical exaggeration = 30x.

Figure 8 – TWT structure maps highlighting the geometry of spiculitic edifices from Horizon H3 to H1. a) Highlights the geometry of isolated (cool-water) build-ups in the Polarrev Formation (Early Permian). b) Denotes the presence of polygonal mounds in the Upper Permian (Røye Formation). c) Highlights the presence of polygonal mounds in Horizon H1, 50-100 ms below the P-T boundary. The maps have a 30x vertical exaggeration.

Figure 9 - Relevant statistical data for the interpreted carbonate build-ups and mounds. a) Plot of thickness vs. interpreted seismic horizons highlighting the variations in the thickness of build-ups and mounds across the study area. Note the thickness maximum for isolated (cool-water) build-ups in the Polarrev Formation and the relatively small variations in thickness recorded by Upper Permian mounds. b) Overlay of the position of build-ups and mounds from H3 to H1, highlighting the marked shifts in their location. c) Overlay of the position of build-ups from H6 to H4, showing once again marked variations in the location of Late Carboniferous build-ups. These changes in the position of the carbonate build-ups and Si-rich mounds are likely to result from a combination of early halokinesis and regional (late Variscan) tectonics.

Figure 10 - Coherence maps highlighting the change in the geometry of Permian build-ups and mounds in the Samson Dome area. a) Coherence slice at Z=3316 ms showing the geometry of isolated carbonate build-ups near the top of the Polarrev Formation (Early Permian). Compare with the time-structural map in Fig. 8a. b) Coherence slice at Z=2996 ms highlighting the existence of mounds ~ 20 m (50-100 ms) below the P-T boundary. The same mounds are shown on the time-structural map in Fig. 8c.

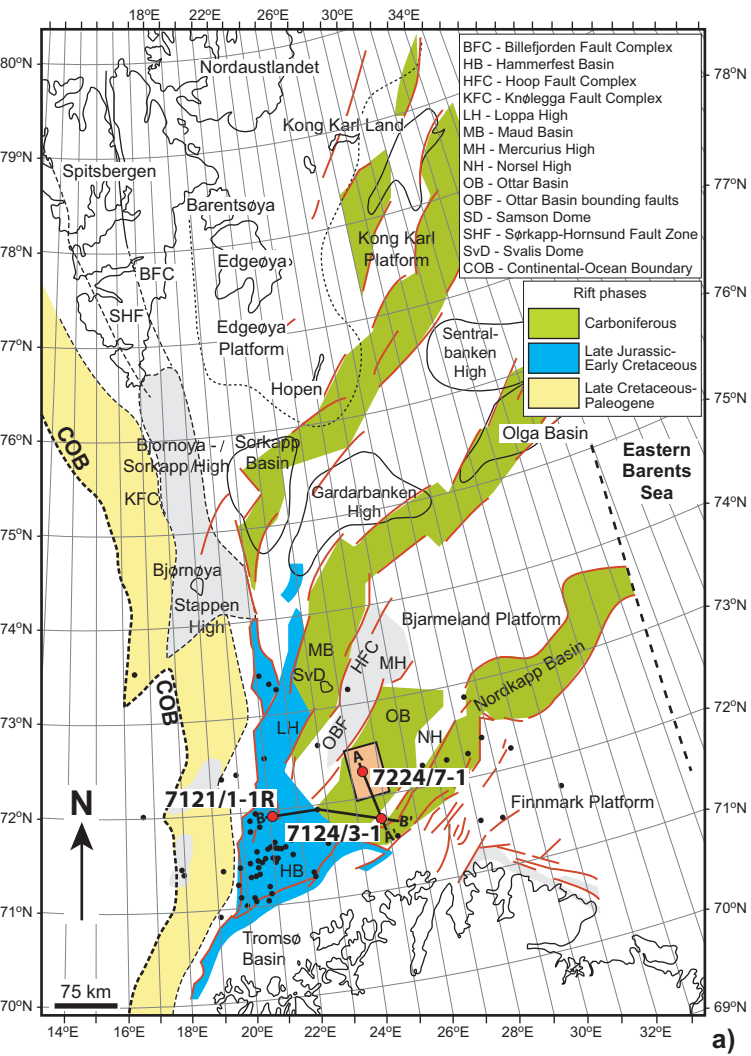
BFC - Billefjorden Fault Complex
HB - Hammerfest Basin
HFC - Hoop Fault Complex
KFC - Knølegga Fault Complex
LH - Loppa High
MB - Maud Basin
MH - Mercurius High
NH - Norsel High
OB - Ottar Basin
OBF - Ottar Basin bounding faults
SD - Samson Dome
SHF - Sørkapp-Hornsund Fault Zone
SvD - Svalis Dome
COB - Continental-Ocean Boundary
Rift phases
Carboniferous
Late Jurassic-Early Cretaceous
Late Cretaceous-Paleogene
Nordaustlandet
Kong Karl Land
Spitsbergen
Barentsøya
Edgeøya
Kong Karl Platform
BFC
SHF
Edgeøya Platform
Sentral-banken High
Hopen
Olga Basin
Eastern Barents Sea
Bjørnøya - / Sørkapp High
Sørkapp Basin
KFC
Gardarbanken High
Bjørnøya
Stappen High
Bjarmeland Platform
MB
SvD
HFC
MH
Nordkapp Basin
LH
OBF
OB
NH
7224/7-1
7121/1-1R
7124/3-1
Finnmark Platform
HB
Tromsø Basin
N
75 km
a)

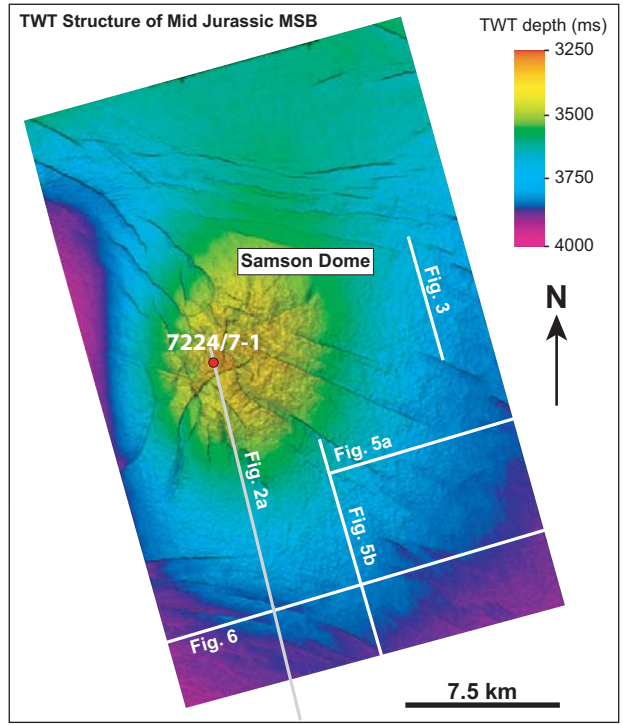
TWT Structure of Mid Jurassic MSB
TWT depth (ms)
3250
3500
3750
4000
Samson Dome
7224/7-1
Fig. 3
Fig. 5a
Fig. 2a
Fig. 5b
Fig. 6
N
7.5 km
b)

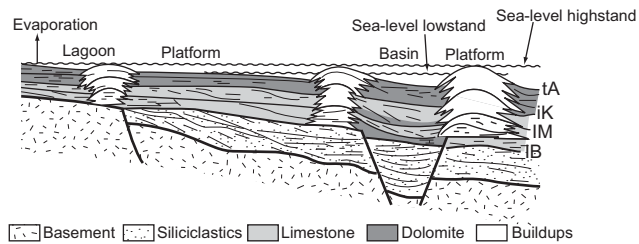
Evaporation
Lagoon
Platform
Sea-level lowstand
Basin
Platform
Sea-level highstand
tA
iK
IM
IB
Basement
Siliciclastics
Limestone
Dolomite
Buildups
c)

Figure 1

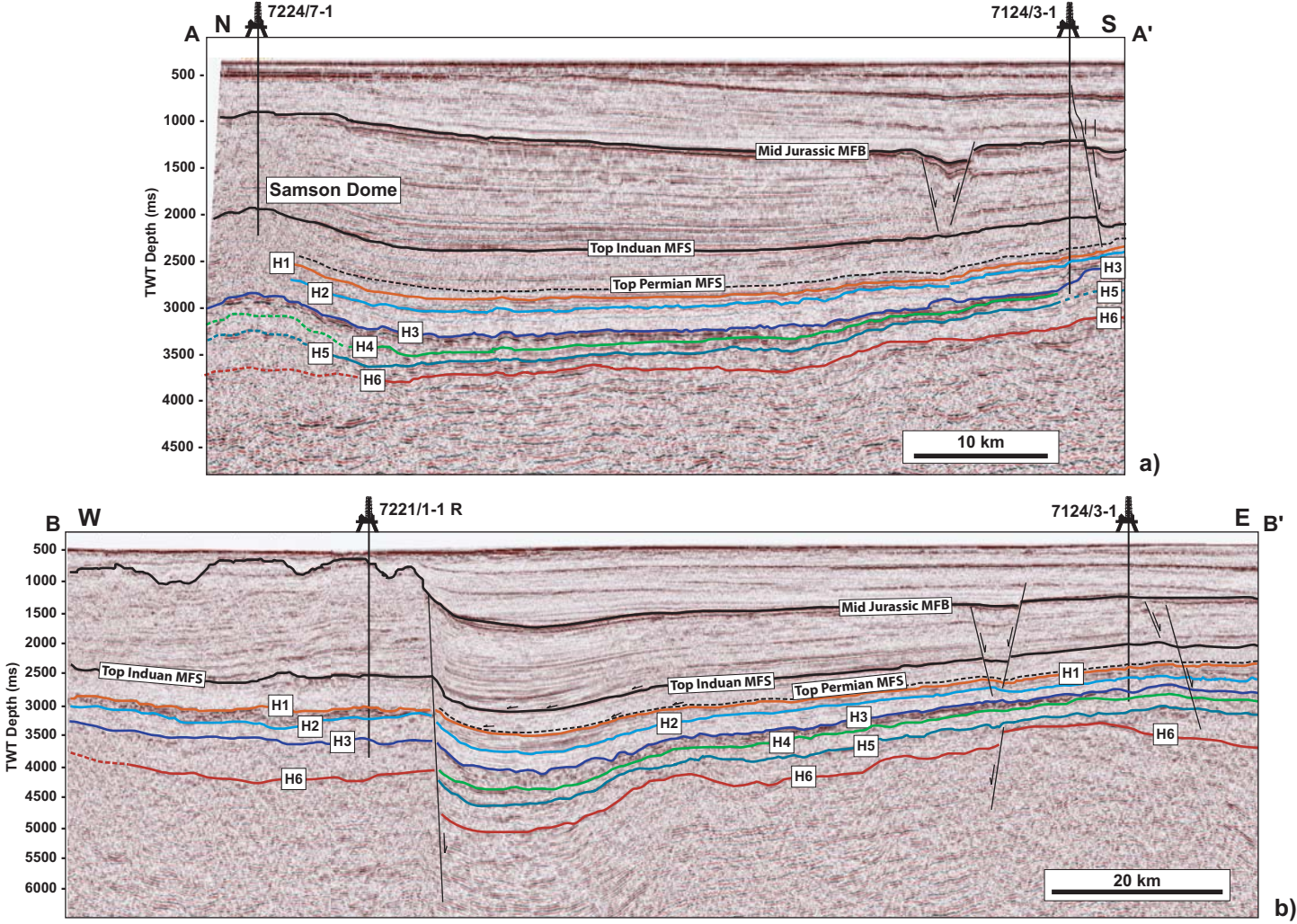
A
N
7224/7-1
7124/3-1
S
A'
TWT Depth (ms)
500
1000
1500
2000
2500
3000
3500
4000
4500
Samson Dome
Mid Jurassic MFB
Top Induan MFS
Top Permian MFS
H1
H2
H3
H4
H5
H6
10 km
a)
B
W
7221/1-1 R
7124/3-1
E
B'
TWT Depth (ms)
500
1000
1500
2000
2500
3000
3500
4000
4500
5000
5500
6000
Top Induan MFS
Mid Jurassic MFB
Top Induan MFS
Top Permian MFS
H1
H2
H3
H4
H5
H6
20 km
b)

Figure 2

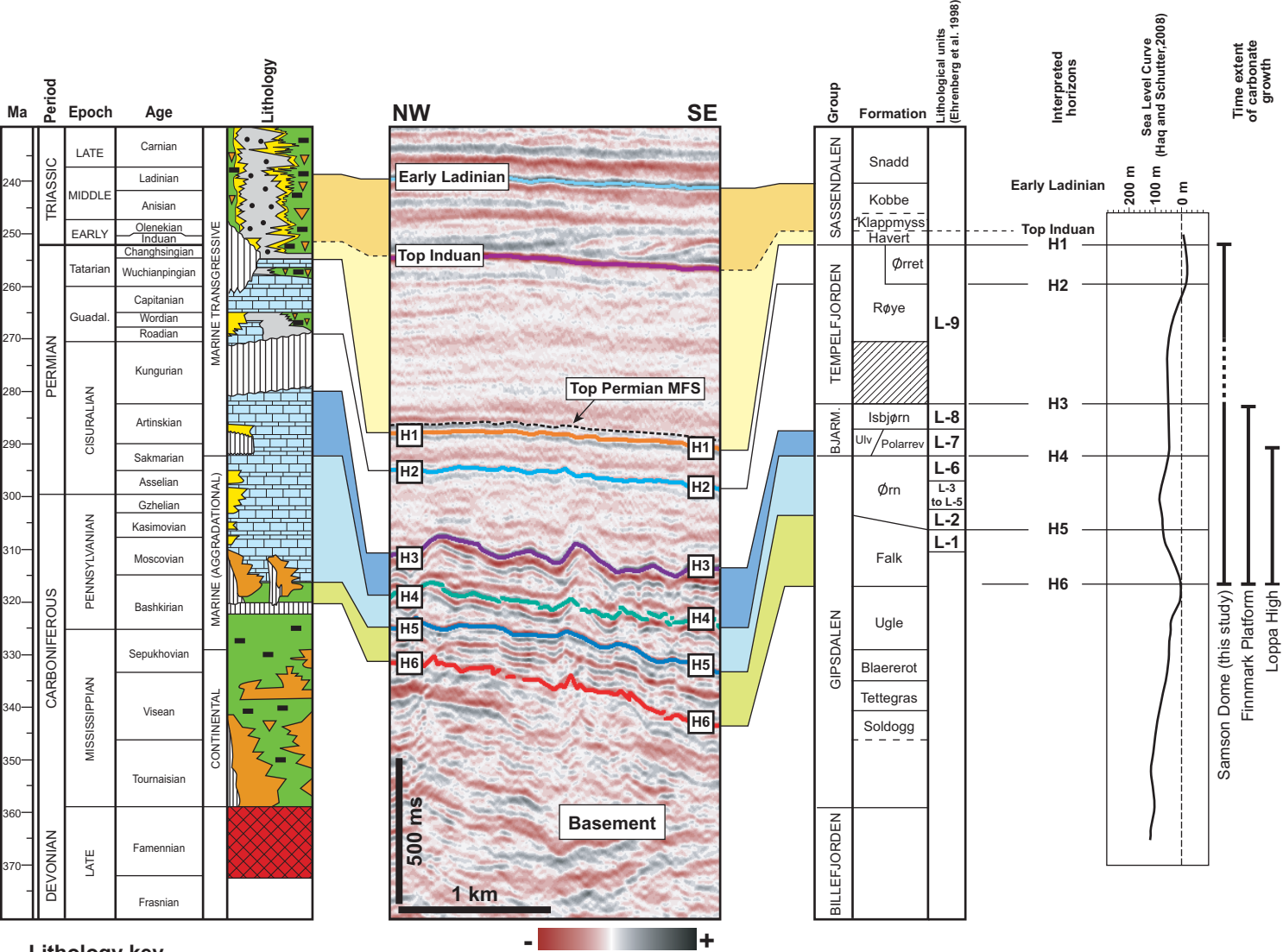

Lithology key

- Continental clay and silt
- Continental sand
- Marine sand
- Marine shale and silt
- Limestone
- Coal
- Chert (spiculite)
- Marine kerogen
- Anhydrite

Figure 3

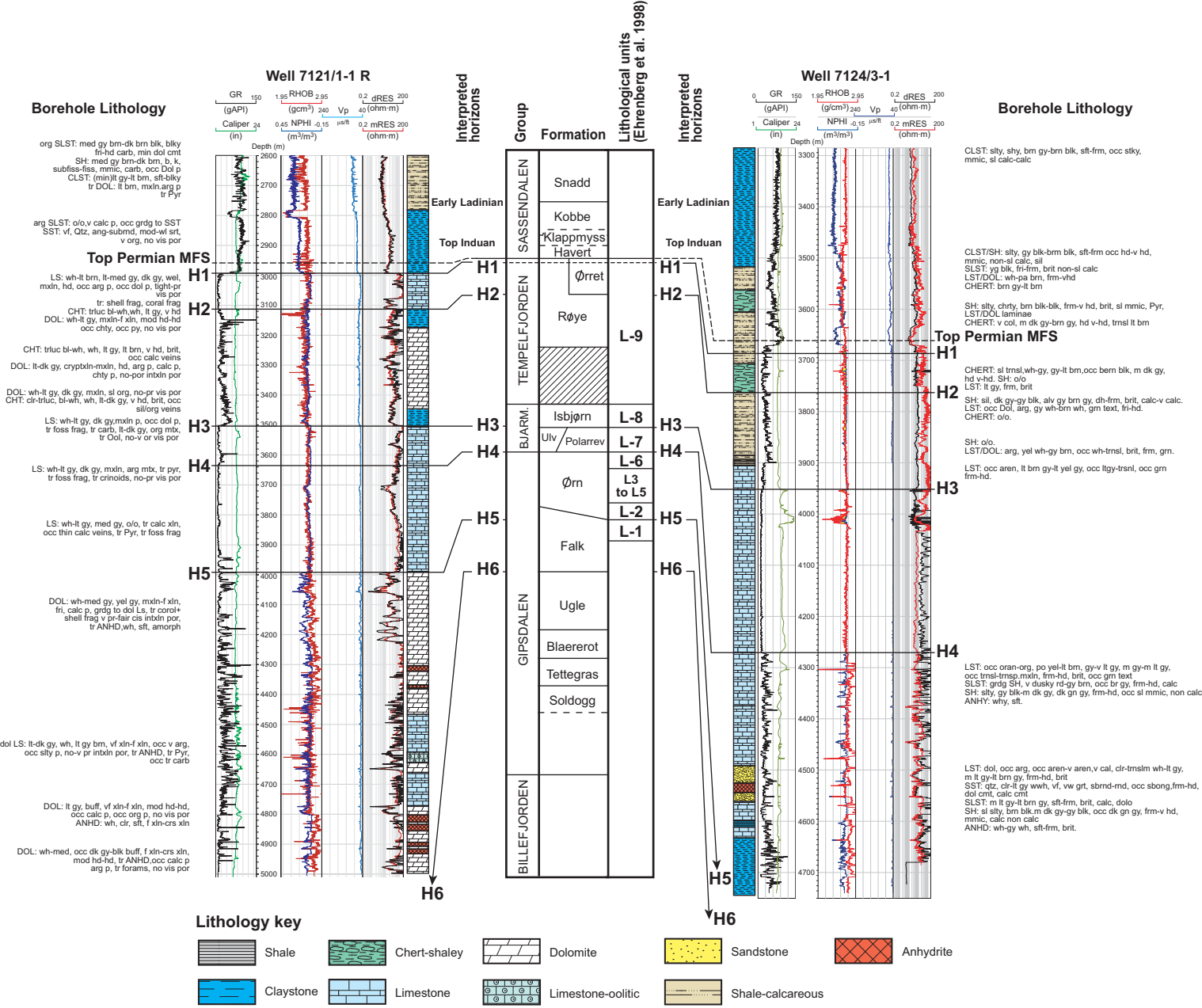
Well 7121/1-1 R
Well 7124/3-1
Borehole Lithology
Borehole Lithology
GR (gAPI)
Caliper (in)
RHOB (gcm3)
NPHI (m3/m3)
Vp
dRES (ohm·m)
mRES (ohm·m)
Depth (m)
Interpreted horizons
Group
Formation
Lithological units (Ehrenberg et al. 1998)
Interpreted horizons
SASSENDALEN
TEMPELFJORDEN
BJARM.
GIPSDALEN
BILLEFJORDEN
Snadd
Kobbe
Klappmyss
Havert
Ørret
Røye
Isbjørn
Ulv
Polarrev
Ørn
Falk
Ugle
Blaererot
Tettegras
Soldogg
L-9
L-8
L-7
L-6
L3 to L5
L-2
L-1
Early Ladinian
Top Induan
Top Permian MFS
H1
H2
H3
H4
H5
H6
org SLST: med gy brn-dk brn blk, blky fri-hd carb, min dol cmt
SH: med gy brn-dk brn, b, k, subfiss-fiss, mmic, carb, occ Dol p
CLST: (min)lt gy-lt brn, sft-blky
tr DOL: lt brn, mxln,arg p
tr Pyr
arg SLST: o/o,v calc p, occ grdg to SST
SST: vf, Qtz, ang-subrnd, mod-wl srt, v org, no vis por
LS: wh-lt brn, lt-med gy, dk gy, wel, mxln, hd, occ arg p, occ dol p, tight-pr vis por
tr: shell frag, coral frag
CHT: trluc bl-wh,wh, lt gy, v hd
DOL: wh-lt gy, mxln-f xln, mod hd-hd
occ chty, occ py, no vis por
CHT: trluc bl-wh, wh, lt gy, lt brn, v hd, brit, occ calc veins
DOL: lt-dk gy, cryptxln-mxln, hd, arg p, calc p, chty p, no-por intxln por
DOL: wh-lt gy, dk gy, mxln, sl org, no-pr vis por
CHT: clr-trluc, bl-wh, wh, lt-dk gy, v hd, brit, occ sil/org veins
LS: wh-lt gy, dk gy,mxln p, occ dol p, tr foss frag, tr carb, lt-dk gy, org mtx, tr Ool, no-v or vis por
LS: wh-lt gy, dk gy, mxln, arg mtx, tr pyr, tr foss frag, tr crinoids, no-pr vis por
LS: wh-lt gy, med gy, o/o, tr calc xln, occ thin calc veins, tr Pyr, tr foss frag
DOL: wh-med gy, yel gy, mxln-f xln, fri, calc p, grdg to dol Ls, tr corol+ shell frag v pr-fair cis intxln por, tr ANHD,wh, sft, amorph
dol LS: lt-dk gy, wh, lt gy brn, vf xln-f xln, occ v arg, occ slty p, no-v pr intxln por, tr ANHD, tr Pyr, occ tr carb
DOL: lt gy, buff, vf xln-f xln, mod hd-hd, occ calc p, occ org p, no vis por
ANHD: wh, clr, sft, f xln-crs xln
DOL: wh-med, occ dk gy-blk buff, f xln-crs xln, mod hd-hd, tr ANHD,occ calc p arg p, tr forams, no vis por
CLST: slty, shy, brn gy-brn blk, sft-frm, occ stky, mmic, sl calc-calc
CLST/SH: slty, gy blk-brn blk, sft-frm occ hd-v hd, mmic, non-sl calc, sil
SLST: yg blk, fri-frm, brit non-sl calc
LST/DOL: wh-pa brn, frm-vhd
CHERT: brn gy-lt brn
SH: slty, chrty, brn blk-blk, frm-v hd, brit, sl mmic, Pyr, LST/DOL laminae
CHERT: v col, m dk gy-brn gy, hd v-hd, trnsl lt brn
CHERT: sl trnsl,wh-gy, gy-lt brn,occ bern blk, m dk gy, hd v-hd. SH: o/o
LST: lt gy, frm, brit
SH: sil, dk gy-gy blk, alv gy brn gy, dh-frm, brit, calc-v calc.
LST: occ Dol, arg, gy wh-brn wh, grn text, fri-hd.
CHERT: o/o.
SH: o/o.
LST/DOL: arg, yel wh-gy brn, occ wh-trnsl, brit, frm, grn.
LST: occ aren, lt brn gy-lt yel gy, occ ltgy-trsnl, occ grn frm-hd.
LST: occ oran-org, po yel-lt brn, gy-v lt gy, m gy-m lt gy, occ trnsl-trnsp, mxln, frm-hd, brit, occ gm text
SLST: grdg SH, v dusky rd-gy brn, occ br gy, frm-hd, calc
SH: slty, gy blk-m dk gy, dk gn gy, frm-hd, occ sl mmic, non calc
ANHY: why, sft.
LST: dol, occ arg, occ aren-v aren,v cal, clr-trnslm wh-lt gy, m lt gy-lt brn gy, frm-hd, brit
SST: qtz, clr-lt gy wwh, vf, vw grt, sbrnd-rnd, occ sbong,frm-hd, dol cmt, calc cmt
SLST: m lt gy-lt brn gy, sft-frm, brit, calc, dolo
SH: sl slty, brn blk,m dk gy-gy blk, occ dk gn gy, frm-v hd, mmic, calc non calc
ANHD: wh-gy wh, sft-frm, brit.
Lithology key
Shale
Chert-shaley
Dolomite
Sandstone
Anhydrite
Claystone
Limestone
Limestone-oolitic
Shale-calcareous

Figure 4

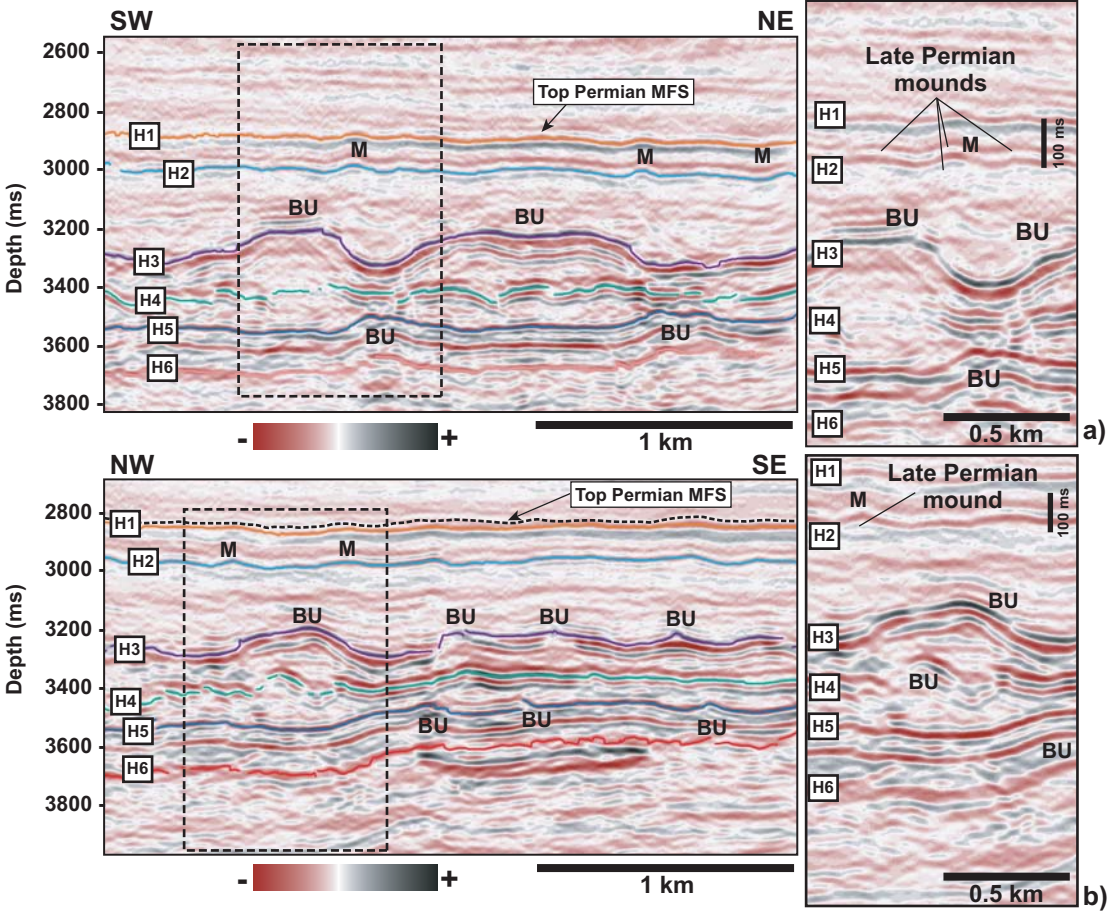
SW
NE
Depth (ms)
2600
2800
3000
3200
3400
3600
3800
Top Permian MFS
H1
H2
H3
H4
H5
H6
M
BU
Late Permian mounds
100 ms
0.5 km
a)
1 km
NW
SE
Late Permian mound
b)

Figure 5

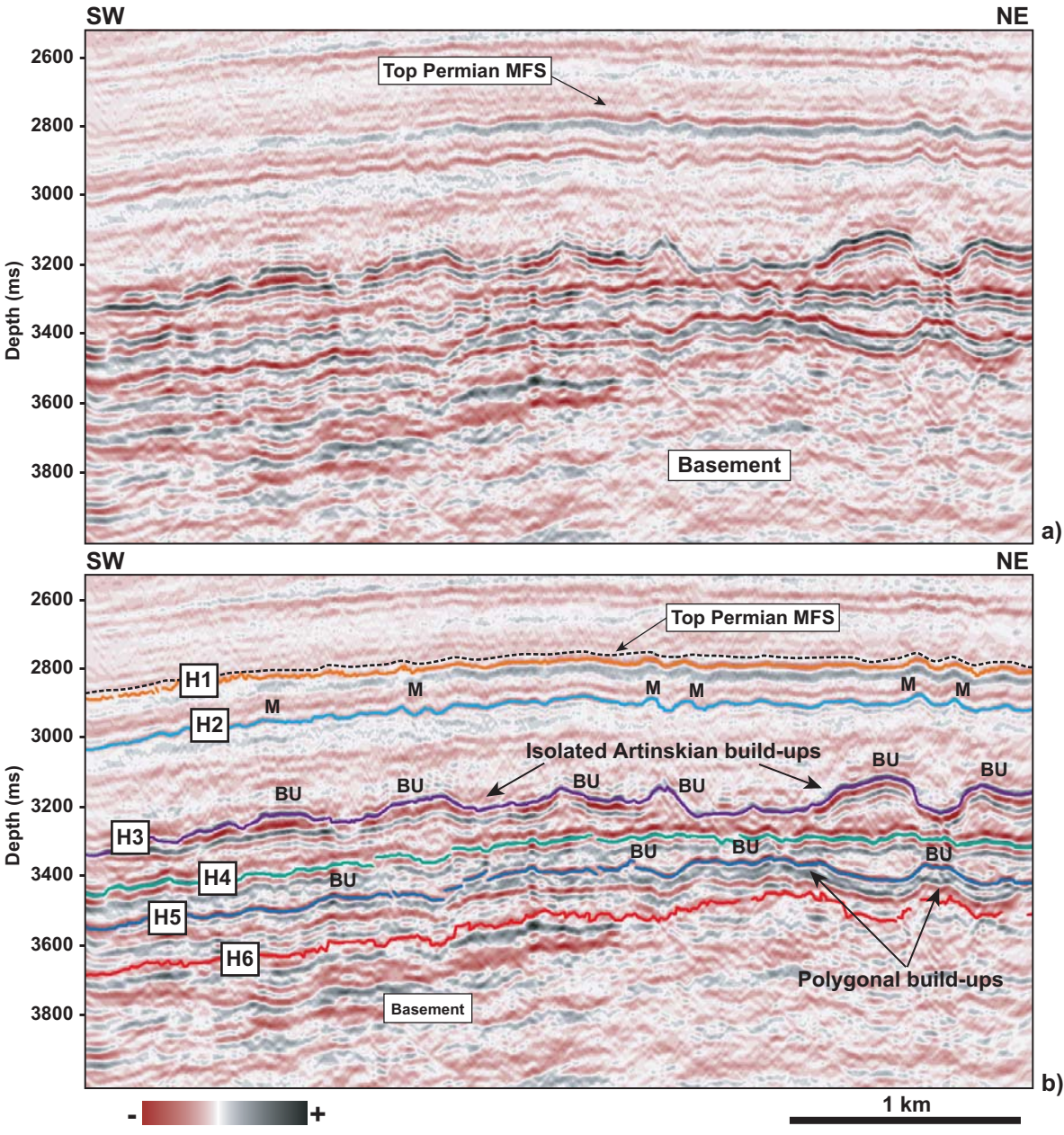
SW
NE
Depth (ms)
2600
2800
3000
3200
3400
3600
3800
Top Permian MFS
Basement
a)
SW
NE
Depth (ms)
Top Permian MFS
H1
H2
H3
H4
H5
H6
M
BU
Isolated Artinskian build-ups
Polygonal build-ups
Basement
b)
-
+
1 km

Figure 6

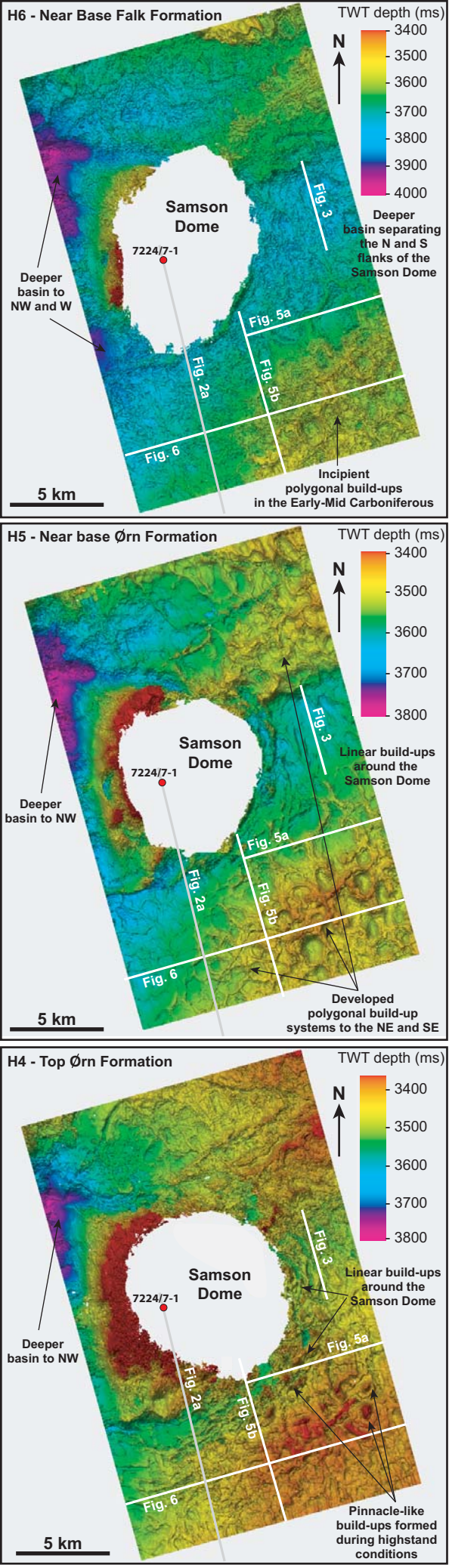
H6 - Near Base Falk Formation
TWT depth (ms)
3400
3500
3600
3700
3800
3900
4000
N
Samson Dome
7224/7-1
Fig. 3
Deeper basin separating the N and S flanks of the Samson Dome
Deeper basin to NW and W
Fig. 5a
Fig. 2a
Fig. 5b
Fig. 6
Incipient polygonal build-ups in the Early-Mid Carboniferous
5 km
a)
H5 - Near base Ørn Formation
TWT depth (ms)
3400
3500
3600
3700
3800
N
Samson Dome
7224/7-1
Fig. 3
Linear build-ups around the Samson Dome
Deeper basin to NW
Fig. 5a
Fig. 2a
Fig. 5b
Fig. 6
Developed polygonal build-up systems to the NE and SE
5 km
b)
H4 - Top Ørn Formation
TWT depth (ms)
3400
3500
3600
3700
3800
N
Samson Dome
7224/7-1
Fig. 3
Linear build-ups around the Samson Dome
Deeper basin to NW
Fig. 5a
Fig. 2a
Fig. 5b
Fig. 6
Pinnacle-like build-ups formed during highstand conditions
5 km
c)

Figure 7

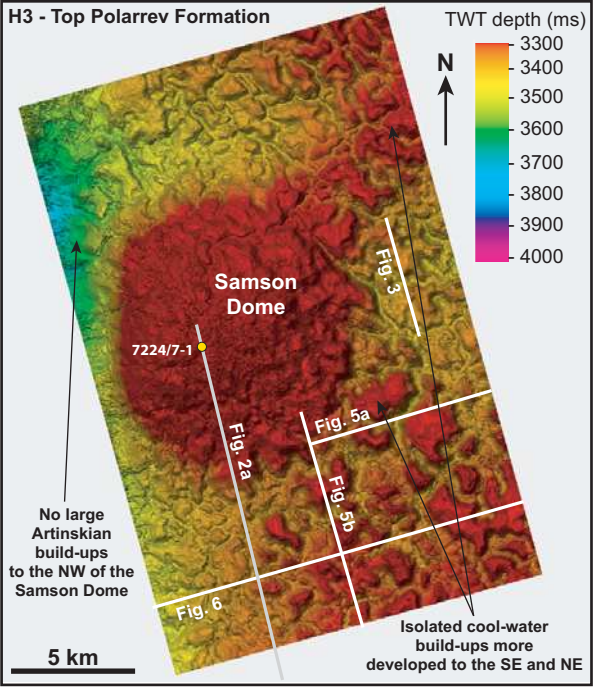
H3 - Top Polarrev Formation
TWT depth (ms)
3300
3400
3500
3600
3700
3800
3900
4000
N
Samson Dome
7224/7-1
Fig. 3
Fig. 2a
Fig. 5a
Fig. 5b
Fig. 6
No large Artinskian build-ups to the NW of the Samson Dome
Isolated cool-water build-ups more developed to the SE and NE
5 km

a)

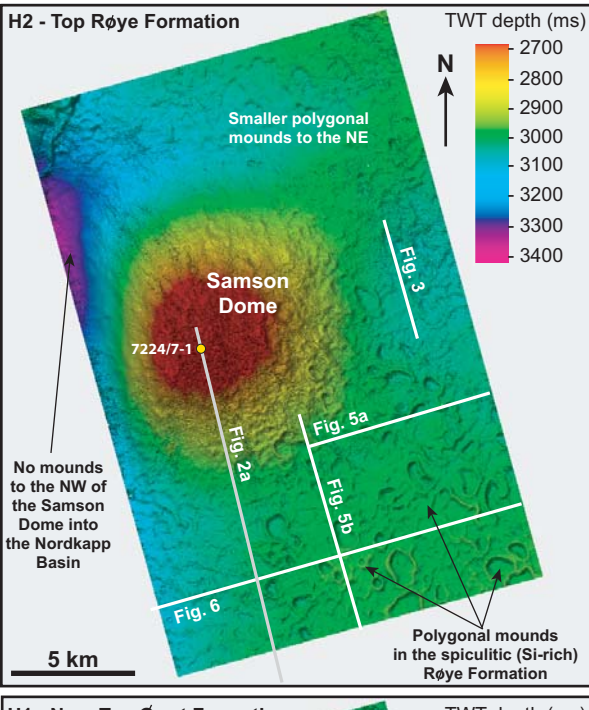
H2 - Top Røye Formation
TWT depth (ms)
2700
2800
2900
3000
3100
3200
3300
3400
N
Smaller polygonal mounds to the NE
Samson Dome
7224/7-1
Fig. 3
Fig. 2a
Fig. 5a
Fig. 5b
Fig. 6
No mounds to the NW of the Samson Dome into the Nordkapp Basin
Polygonal mounds in the spiculitic (Si-rich) Røye Formation
5 km

b)

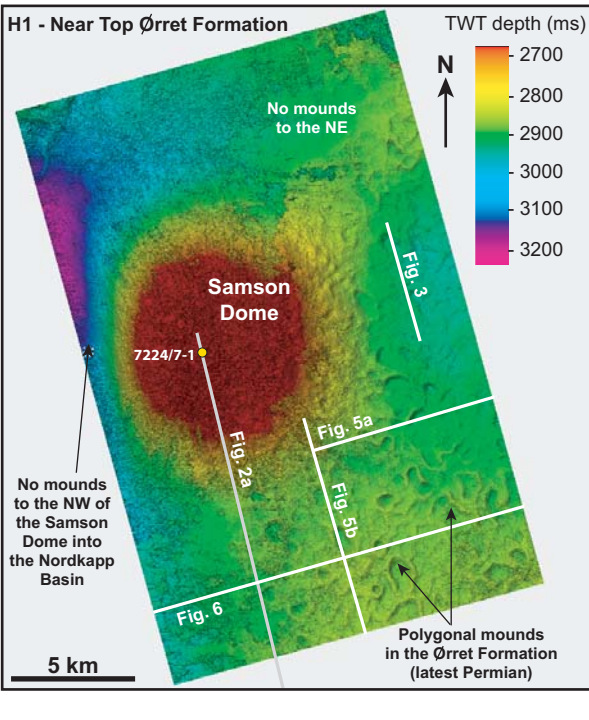
H1 - Near Top Ørret Formation
TWT depth (ms)
2700
2800
2900
3000
3100
3200
N
No mounds to the NE
Samson Dome
7224/7-1
Fig. 3
Fig. 2a
Fig. 5a
Fig. 5b
Fig. 6
No mounds to the NW of the Samson Dome into the Nordkapp Basin
Polygonal mounds in the Ørret Formation (latest Permian)
5 km

c)

Figure 8

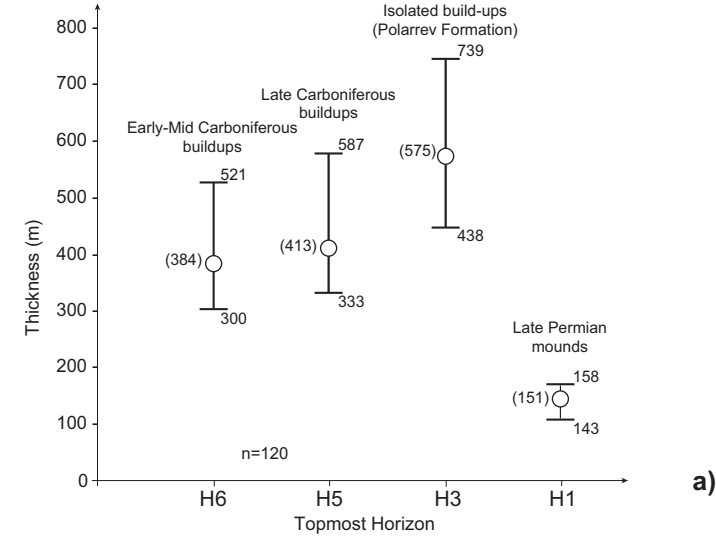
Isolated build-ups
(Polarrev Formation)
739
Late Carboniferous
buildups
Early-Mid Carboniferous
buildups
587
521
(575)
(413)
(384)
438
333
300
Late Permian
mounds
158
(151)
143
n=120
Thickness (m)
800
700
600
500
400
300
200
100
0
H6
H5
H3
H1
Topmost Horizon
a)

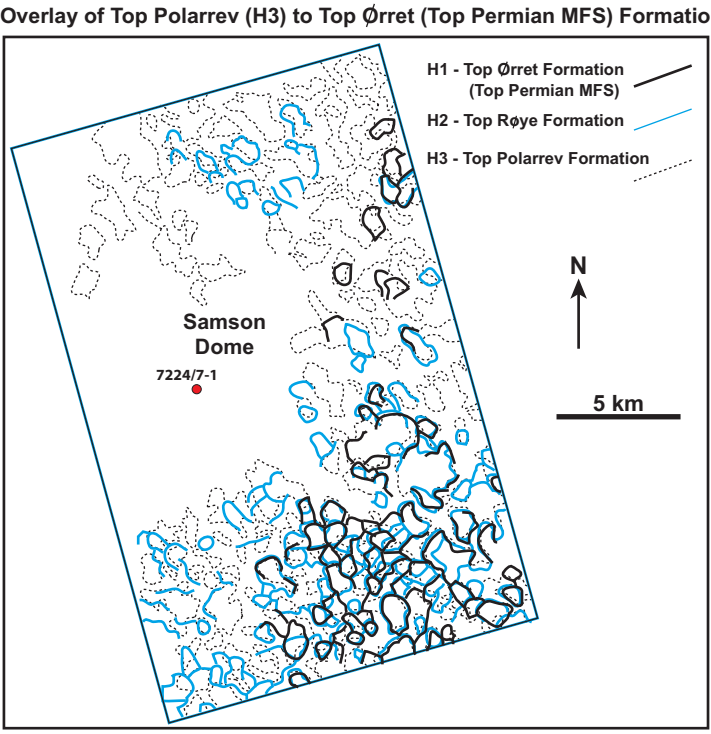
Overlay of Top Polarrev (H3) to Top Ørret (Top Permian MFS) Formations
H1 - Top Ørret Formation
(Top Permian MFS)
H2 - Top Røye Formation
H3 - Top Polarrev Formation
Samson
Dome
7224/7-1
N
5 km
b)

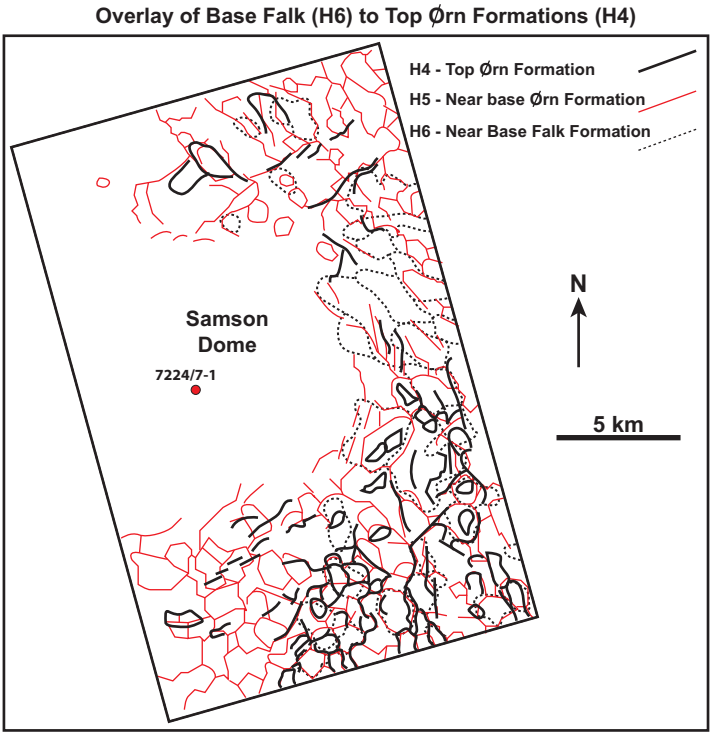
Overlay of Base Falk (H6) to Top Ørn Formations (H4)
H4 - Top Ørn Formation
H5 - Near base Ørn Formation
H6 - Near Base Falk Formation
Samson
Dome
7224/7-1
N
5 km
c)

Figure 9

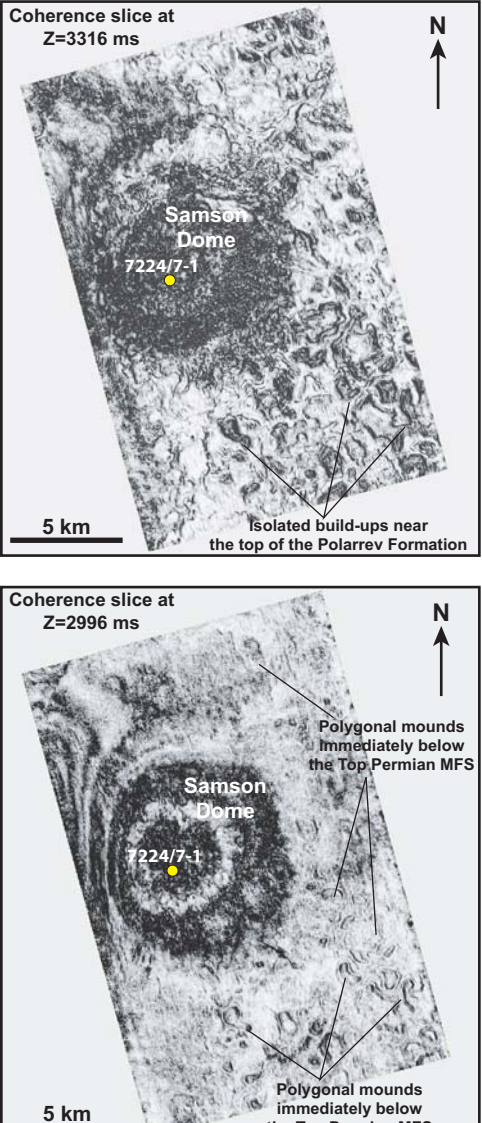
Coherence slice at
Z=3316 ms
N
Samson
Dome
7224/7-1
5 km
Isolated build-ups near
the top of the Polarrev Formation
a)
Coherence slice at
Z=2996 ms
N
Polygonal mounds
Immediately below
the Top Permian MFS
Samson
Dome
7224/7-1
Polygonal mounds
immediately below
the Top Permian MFS
5 km
b)

Figure 10

Unit	Depositional setting and lithology	Age	Average Thickness (m)
L-9	Deep-water spiculite, limestone and spiculitic mud	?Kungurian-Late Permian	129
L-8	Open-shelf limestone	Late Sakmarian-late Artinskian	97
L-7	Offshore to lower-shoreface shale and shallow-water limestone	early Sakmarian	30
L-6	Shallow-shelf limestone	middle Asselian-early Sakmarian	39
L-5	Lagoon/sabkha dolomitic mudstone and shallow-water packstone	middle Asselian	34
L-4	Shallow-water wackestone and buildups (partly dolomitised)	late Gzhelian-early Asselian	76
L-3	Lagoon/sabkha dolomitic mudstone	middle-late Gzhelian	25
L-2	Offshore to lower-shoreface shale, siltstone, and silty limestone	Kasimovian-early Gzhelian	46
L-1	Shallow-water sandstone (partly dolomitised) and limestone	late Moscovian	35

Table 1